

Article

Tetrabromoethane as σ -Hole Donor toward Bromide Ligands: Halogen Bonding between $C_2H_2Br_4$ and Bromide Dialkylcyanamide Platinum(II) Complexes

Anna M. Cheranyova  and Daniil M. Ivanov * 

Institute of Chemistry, Saint Petersburg State University, 199034 Saint Petersburg, Russia; st063368@student.spbu.ru

* Correspondence: d.m.ivanov@spbu.ru

Abstract: The complexes *trans*-[PtBr₂(NCNR₂)₂] (R₂ = Me₂ **1**, (CH₂)₅ **2**) were cocrystallized with 1,1,2,2-tetrabromoethane (**tbe**) in CH₂Cl₂ forming solvates **1**·**tbe** and **2**·**tbe**, respectively. In both solvates, **tbe** involved halogen bonding, viz. the C–Br···Br–Pt interactions, were detected by single-crystal X-ray diffractions experiments. Appropriate density functional theory calculations (M06/def2-TZVP) performed for isolated molecules and complex-**tbe** clusters, where the existence of the interactions and their noncovalent nature were confirmed by electrostatic potential surfaces ($\rho = 0.001$ a.u.) for isolated molecules, topology analysis of electron density, electron localization function and HOMO-LUMO overlap projections for clusters.

Keywords: tetrabromoethane; halogen bonding; platinum(II); dialkylcyanamides



Citation: Cheranyova, A.M.; Ivanov, D.M. Tetrabromoethane as σ -Hole Donor toward Bromide Ligands: Halogen Bonding between $C_2H_2Br_4$ and Bromide Dialkylcyanamide Platinum(II) Complexes. *Crystals* **2021**, *11*, 835. <https://doi.org/10.3390/cryst11070835>

Academic Editor: Sergiy Rosokha

Received: 4 July 2021

Accepted: 17 July 2021

Published: 20 July 2021

Publisher's Note: MDPI stays neutral with regard to jurisdictional claims in published maps and institutional affiliations.



Copyright: © 2021 by the authors. Licensee MDPI, Basel, Switzerland. This article is an open access article distributed under the terms and conditions of the Creative Commons Attribution (CC BY) license (<https://creativecommons.org/licenses/by/4.0/>).

1. Introduction

In the past decade, the halogen bonding (XB) concept [1] has attracted a considerable attention as a new type of intermolecular interaction and has now become an important tool for XB involving crystal engineering. The expressed directionality of XB was subsequently used in biology and materials sciences to create functional systems with a wide range of applications spanning from supramolecular chemistry, to crystal engineering, catalysis, electrochemistry, etc. [2–6]. Although the vast majority of XB studies do not utilize organometallic building blocks, these metal-containing species functioning as XB participants are very useful for the design of new supramolecular systems [7–10].

Involvement of various haloalkanes (in particular bromoalkanes) in the occurrence of XBs is among rapidly growing areas of XB based crystal engineering [3]. Perfluorinated bromoalkanes were found [11–13] to form XBs with metal-free halide anions. Dibromomethane [14,15], bromoform [16,17], tetrabromomethane [16,18,19] and hexabromoethane [20], functioning as XB acceptors, were studied toward halide ligands in metal complexes.

1,1,2,2-tetrabromoethane (**tbe**), which contains the same CHBr₂ fragments as those in dibromomethane or bromoform, have never been utilized as XB donor (Figure 1). This compound is used in organic chemistry as an alkylating agent [21,22] and in ferrocene chemistry as a mild brominating agent [23–27]. The only **tbe** solvates were obtained [28], but they were only characterized by elemental analyses.

In this study, the dialkylcyanamide platinum(II) complexes *trans*-[PtBr₂(NCNR₂)₂] (R₂ = Me₂ **1**, (CH₂)₅ **2**), which function as useful XB acceptors [18,29], were employed as XB acceptors toward **tbe** (Figure 1). Since **tbe** may be a source of bromides, the bromide complexes were chosen in order to exclude various exchange reactions between the halogens.

We report herein our data on cocrystallization of **tbe** with dialkylcyanamide bromide complexes of platinum (II). In 1:1 solvates **1**·**tbe** and **2**·**tbe**, the first examples of **tbe** involved XBs and hydrogen bonds (HBs) were found.

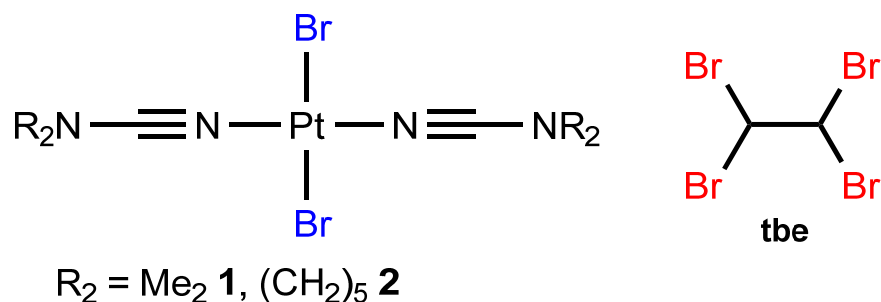


Figure 1. Studied XB partners.

2. Materials and Methods

1,1,2,2- $\text{C}_2\text{H}_2\text{Br}_4$, $\text{K}_2[\text{PtCl}_4]$, KBr, dialkylcyanamides and all solvents were obtained from commercial sources and used as received; complex *trans*- $[\text{PtBr}_2(\text{NCNMe}_2)_2]$ (**1**) was synthesized via a previously published procedure [29].

2.1. Synthesis of Complex *Trans*- $[\text{PtBr}_2(\text{NCN}(\text{CH}_2)_5)_2]$

To $\text{K}_2[\text{PtCl}_4]$ (0.1 g, 0.24 mmol) in water (1 mL) added a 10-fold excess of KBr (0.284 g, 2.4 mmol), whereupon the solution was heated with mixing for 2 h at 70 °C. After heating the solution became maroon. A 5-fold excess of $\text{NCNC}_5\text{H}_{10}$ (0.140 mL, 1.2 mmol) was added to this solution. Oil formed at the bottom of the vessel after 24 h. The resulting oil was powdered with diethyl ether and held under ultrasound. The resulting precipitate (a mixture of *cis*- and *trans*-isomers) was washed with three portions of 3 mL of water and diethyl ether, and then dried in air at room temperature. To isolate the pure *trans*-isomer, the resulting mixture was dissolved in CHCl_3 and was refluxed for 3 h. Yield: 71%. ^1H NMR (400 MHz, CDCl_3) $\delta = 3.32$ (m, NCH_2), 1.62–1.67 (m, NCH_2CH_2) and 1.52–1.59 (m, $\text{NCH}_2\text{CH}_2\text{CH}_2$) ppm (Figure S5). $^{13}\text{C}\{^1\text{H}\}$ NMR (101 MHz, CDCl_3) $\delta = 115.74$ (s, $\text{C}\equiv\text{N}$), 49.79 (s, NCH_2CH_2), 24.53 (s, $\text{CH}_2\text{CH}_2\text{CH}_2$) and 22.48 (s, $\text{CH}_2\text{CH}_2\text{CH}_2$) ppm (Figure S6). ^{195}Pt NMR (86 MHz, CDCl_3) $\delta = -2596.15$ ppm (Figure S7). HRESI-MS, m/z : calculated for $[\text{M}+\text{H}]^+$ 576.9732, found 576.9755 (Figure S4). Single crystals of **2** were prepared from a dichloromethane at RT by slow evaporation (Figure S1). Comparison of the XRD and PXRD data showed that the phases coincide (Figure S8).

2.2. Crystallization

Single crystals of **1**·**tbe** and **2**·**tbe** were obtained by slow evaporation of a dichloromethane solution (1 mL) of a mixture of the corresponding **1** (0.002 mmol) or **2** (0.002 mmol) and **tbe** taken in an excess (0.87 mmol) at RT. Yellow crystals **2**, **1**·**tbe** and **2**·**tbe** of suitable for XRD were released after 3–4 d.

2.3. Analytic Methods

The MS data were obtained on a Bruker micrOTOF spectrometer equipped with electrospray ionization (ESI) source. The NMR spectra were recorded on a Bruker AVANCE III 400 spectrometer at ambient temperature in CDCl_3 (at 400, 101, 86 MHz for ^1H , $^{13}\text{C}\{^1\text{H}\}$ and ^{195}Pt NMR spectra, respectively). IR spectra were recorded on a Bruker TENSOR 27 FT-IR spectrometer ($4000\text{--}200\text{ cm}^{-1}$, KBr pellets) (Figure S3). Powder X-ray diffraction (PXRD) data were measured at room temperature using a Bruker D2 Phaser Desktop X-ray diffractometer equipped with a $\text{CuK}\alpha 1 + 2$ source; the data were collected in the range of $2\theta = 5\text{--}80^\circ$ with a step size of $0.02^\circ (2\theta)$.

2.4. X-ray Structure Determination and Refinement

Suitable single crystals were studied on a SuperNova Duo CCD diffractometer ($\text{Cu K}\alpha$ ($\lambda = 1.54184$), mirror monochromator, ω -scan). Crystals were incubated at 100 K during data collection. All structures were deciphered by direct methods using SHELXT [30] and refined using SHELXL [31]. All non-hydrogen atoms were refined with individual

parameters of anisotropic displacement. Hydrogen atoms in all structures are placed in ideal calculated positions and refined as colliding atoms with parameters of relative isotropic displacement. The main data of crystallography and details of refinement are given in Table S1 in Supporting Information. CCDC numbers 2094282–2094284 contain all supporting structural and refinement data.

2.5. Computational Details

The energy characteristics of the complexes, *tbe* and clusters included in this study were calculated by the DFT method with the M06/def2-TZVP [32,33] theory using atom coordinates obtained from crystal structures. The GAUSSIAN-09 [34] program was used for calculations. The MEP surfaces [35] were calculated at the same theoretical level and presented using 0.001 a.u. isosurfaces. The color scheme is a red-white-blue scale with red for $\rho+$ cut (repulsive) and blue for $\rho-$ cut (attractive). White isosurfaces correspond to weakly repulsive and attractive interactions, respectively. 3D-surfaces were visualized using the VMD 1.9.3 [36] program. ELF projections and QTAIM analysis was performed in Multiwfn 3.7 [37,38] software. The QTAIM analysis was performed using the program at the same level of theory. Visualization of the projections of boundary orbitals was carried out using the program Multiwfn 3.7.

3. Results and Discussion

3.1. Electrostatic Surface Potentials

Electrostatic potentials (ESP) on surface ($\rho = 0.001$ a.u.) were calculated (M06/def2-TZVP) for *tbe*, **1** and **2** isolated molecules. Donor XB has a σ -hole on the surface of the bromine atom, which we see for *tbe* (positive potential, Figure 2). XB acceptors are nucleophiles, and bromide ligands demonstrate significant negative potential on all sides (Figure 3). The scale was selected in such a way as to convey as much information as possible about the distribution of the electrostatic potential in the molecules [39,40]. Thus, the ESP calculations show that the formation of XB and HB is promising for their joint crystallization.

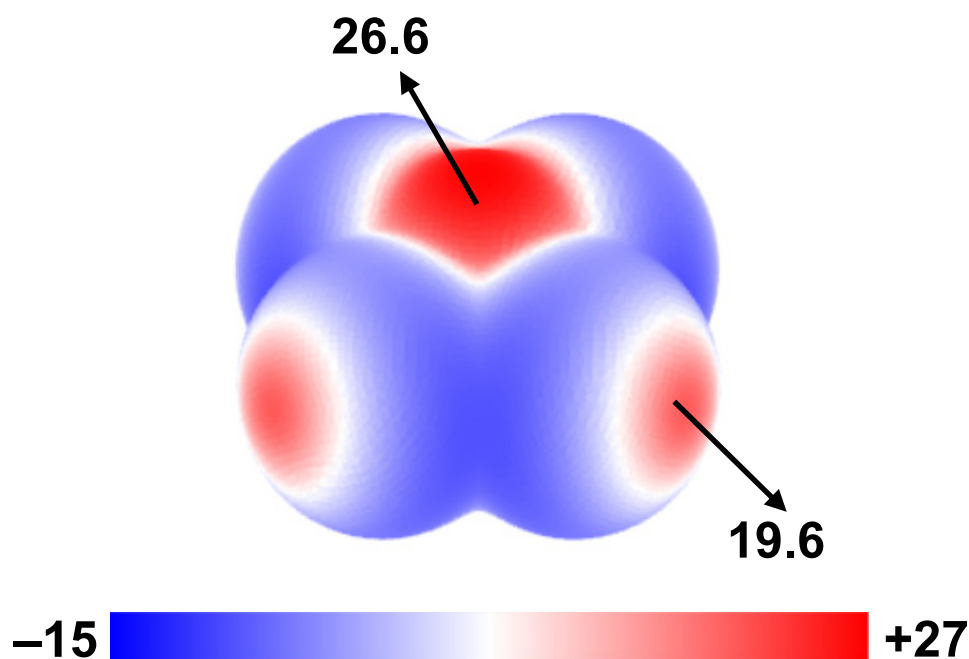


Figure 2. ESP on surface ($\rho = 0.001$ a.u.) for *tbe* in kcal/mol.

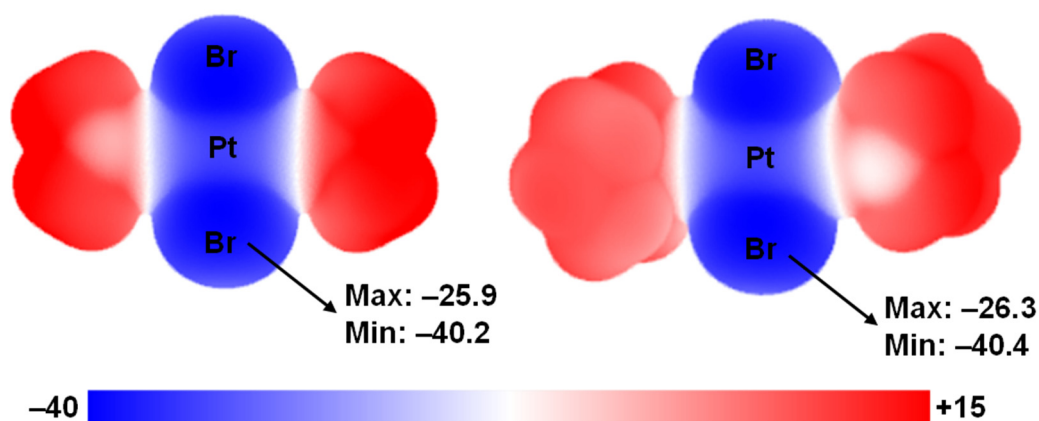


Figure 3. ESP on surface ($\rho = 0.001$ a.u.) for 1 and 2 in kcal/mol.

3.2. Single-Crystal X-ray Diffraction Data for Solvates

The structure of **1**·**tbe** consists of one molecule of the complex *trans*-[PtBr₂(NCNMe₂)₂] and one molecule of **tbe**; the same is observed in the structure of adduct **2**·**tbe**. In both cases, the complex molecule is surrounded by 4 **tbe** molecules with the formation of bromine–bromine short contacts.

For the **1**·**tbe** structure (Figure 4a), these contacts are 3.3734(12) Å and 3.4613(16) Å, which are less than $2R_{\text{vdW}}(\text{Br}) = 3.70$ Å [41], and the angle around bromine is close to 180° (173.8(3)° and 174.3(3)°). For structure **2**·**tbe** (Figure 4b), the distances between bromine and bromide ligand are 3.5585(7) Å and 3.6100(7) Å, and the angles are close to 180° (167.20(13)° and 174.56(13)°). All the angles around bromide ligands are far from linear (Table 1), and the C–Br···Br–Pt interactions can be treated as type II halogen–halogen contacts, i.e., XBs [42].

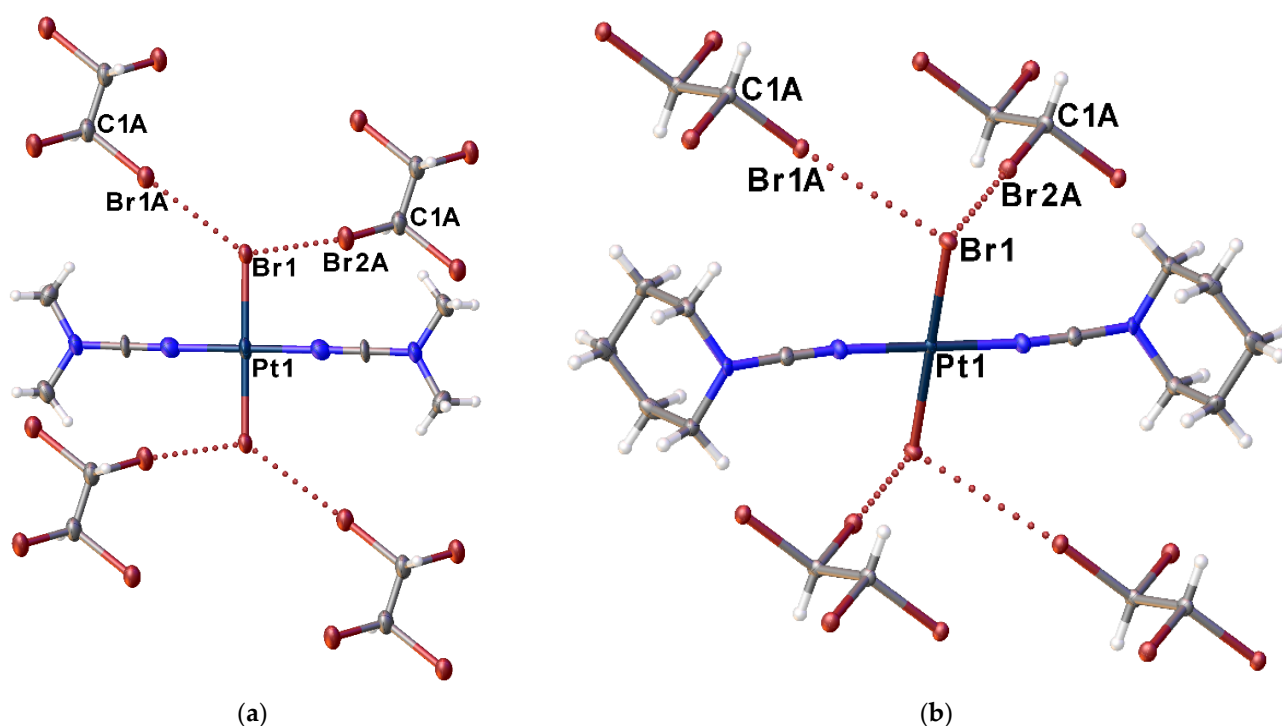


Figure 4. (a) the environment of 1 in **1**·**tbe**, halogen bonds assigned by dotted lines. Hereinafter thermal ellipsoids are shown with 50% probability; (b) The environment of 2 in **2**·**tbe**, halogen bonds assigned by dotted lines.

Table 1. Parameters of XB in adducts **1·tbe** and **2·tbe** (X = 1, 2).

Solvate	$d(\text{BrXA}\cdots\text{Br1}), \text{Å}$	$\angle(\text{C1A}-\text{BrXA}\cdots\text{Br1}), ^\circ$	$\angle(\text{BrXA}\cdots\text{Br1}-\text{Pt1}), ^\circ$
1·tbe	3.3734 (12)	173.8 (3)	124.19 (4)
	3.4613 (16)	174.3 (3)	93.48 (3)
2·tbe	3.5585 (7)	167.20 (13)	112.284 (17)
	3.6100 (7)	174.56 (13)	87.635 (14)

In **1·tbe**, when the halogen bonds are stronger, a significant (within 3σ) elongation of the Pt–Br coordination bonds (2.4340(6) Å and 2.4555(9) Å) is observed, which can be explained by the redistribution of the electron density during the formation of these halogen bonds. In **2·tbe**, there is no difference within 3σ in the isolated molecule (2.4382(6) Å) and in the solvate (2.4357(4) Å). However, there is a difference in the piperidyl conformations in the solvent-free crystal **2** and in **2·tbe**, which can be explained by the crystal packing effects.

By analogy with the formation of two XBs with a bromide ligand, the formation of two HBs with sterically available oxygen in the composition of phosphine oxide is possible, which shows the general behavior between different supramolecular synthons [43].

The formation of XBs leads to the 2D supramolecular layers in both cases (Figure S2). In **1·tbe**, the additional $\text{Br}_2\text{CHCBr}_2\text{-H}\cdots\text{Br-Pt}$ hydrogen bonds were detected (Figure S9 and Table S2). The hydrogen bonds together with XBs allow the 3D scaffold supramolecular structure of **1·tbe**.

3.3. Theoretical Consideration

In addition to ESP surfaces, the presence and nature of intermolecular interactions were studied using the complex·**tbe** clusters with each type (see Supplementary Materials for details) of the interactions under consideration. The calculation (M06/def2-TZVP) was carried out on the experimentally obtained atomic coordinates. To obtain more information about the weak interactions under study, a topological analysis of the electron density distribution was carried out within the framework of the Bader QTAIM method [44,45].

The QTAIM analysis demonstrates the presence of a bond critical point (3, −1) (BCP) between the bromine and the bromide ligand (Table 2), as well as between the bromine in **tbe** and the hydrogen atoms in the complexes. Negative [46] and small values of $\text{sign}(\lambda_2)\rho$ at the BCPs confirm the attractive and noncovalent nature of the interactions. They can also be treated as typically noncovalent due to close to zero positive energy density (0.001–0.002 a.u.) and the balance of the Lagrangian kinetic energy $G(r)$ and the potential energy density $V(r)$ ($-G(r)/V(r) > 1$) on the corresponding BCPs.

Table 2. Potential energy density $V(r)$, Lagrangian kinetic energy $G(r)$ and energy density $H(r)$ (Hartree) at the bond critical points (3, −1), sums of NPA atomic charges on *tbe* ($\Sigma_{\text{NPA}}(\text{tbe})$, in q_e), and values of the Wiberg indices (WBI), corresponding to different noncovalent interactions in **1·tbe** and **2·tbe**.

Cluster	XB	$\text{Sign}(\lambda_2)\rho$	$G(r)$	$V(r)$	$H(r)$	$\Sigma_{\text{NPA}}(\text{tbe})$	WBI
(1)·(tbe) (type 1)	Br1A \cdots Br1	−0.012	0.008	−0.006	0.002	−0.033	0.04
(1)·(tbe) (type 2)	Br2A \cdots Br1	−0.011	0.007	−0.006	0.001	−0.026	0.03
(2)·(tbe) (type 1)	Br1A \cdots Br1	−0.009	0.005	−0.004	0.001	−0.016	0.02
(2)·(tbe) (type 2)	Br2A \cdots Br1	−0.008	0.005	−0.004	0.001	−0.015	0.02

The same calculations for the same clusters were performed in natural atomic partitioning scheme. The sums of natural population analysis (NPA) atomic charges are negative on the **tbe** molecule in each cluster, so the interaction between halogens also occurs due to the charge transfer from the complex molecules to **tbe**. Wiberg bond indices in NPA can be interpreted as chemical bond indices (orders). In all clusters, the Wiberg bond indices of

the Br \cdots Br XBs are very small but not zero (0.02–0.04) which point to the small covalent contribution to these interactions.

The ELF is a derivative of the electron density, which allows the location of areas of shared and unshared electron pairs [18,47–49]. A combination of ELF and QTAIM methods is represented in Figure 5, where ELF projections were plotted together with bond (3, –1) critical points (BCPs, blue), nuclear (3, –3) critical points (NCPs, brown), ring (3, +1) critical points (RCPs, orange), and bond paths (white lines).

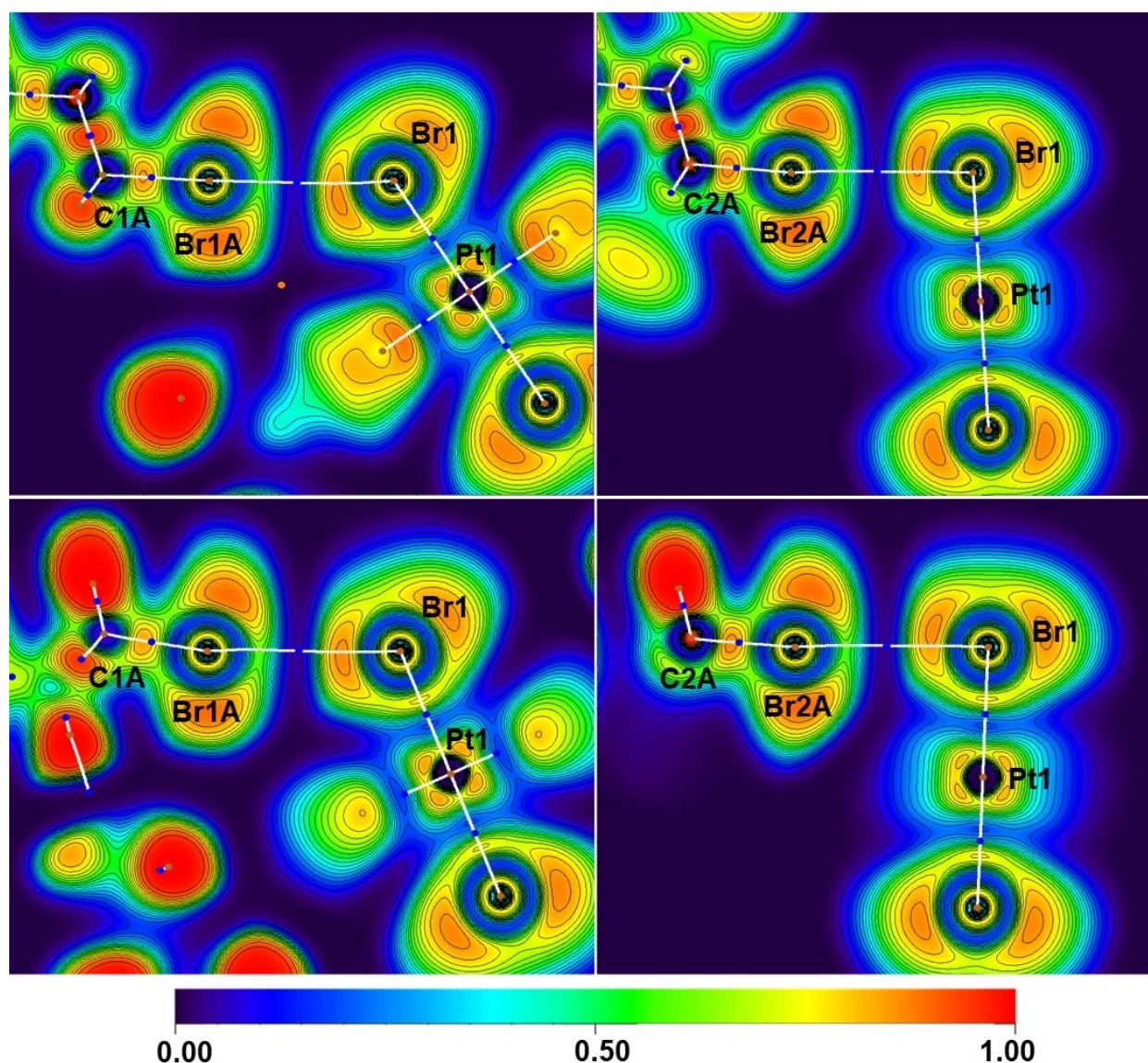


Figure 5. ELF projection and bond paths (white lines), BCPs (blue dots), NCPs (brown dots) and RCPs (orange dots) for the C1A–Br1A \cdots Br1–Pt1, C1A–Br2A \cdots Br1–Pt1 XBs in **1·tbe** and **2·tbe**.

In **(1)·(tbe)** clusters, the Br \cdots Br bond paths (top on Figure 5) pass through the lone pairs of bromide and through the depletion ELF areas of the on bromine atoms in **tbe**. These observations confirm the XB nature of the Br \cdots Br interactions, where bromide ligands are nucleophiles and **tbe** molecules are electrophiles.

The same observations were performed for **(2)·(tbe)** clusters (bottom on Figure 5) halogen-bonding bond paths go through lone pairs on the halide ligands and the σ -holes on Br atoms in XB donors.

It is noteworthy that, in the case of these clusters the ELF regions for halogen bonding Br1A \cdots Br1 and Br2A \cdots Br1, the critical points of bonds and the arrangement of bond paths

are the same for both clusters, which indicates the similarity in the nature of noncovalent interactions.

Intermolecular halogen bonds are always directed towards their bromide ligands. It should be noted that the HOMO's of the complex are located mainly on bromide ligands. The superposition of the boundary orbitals of donors and acceptors of halogen bonds on the crystal structures of their adducts demonstrates that all associates exhibit HOMO/LUMO overlaps (Figure 6) [12,16,50]. To construct the projections, HOMO-1 was taken, since the lone pairs of the bromine atom are in the plane of the complex, and for HOMO they are perpendicular to the plane. HOMO-LUMO overlap projections were built along with the construction of connection paths. This suggests that the arrangement of Br...Br contacts is associated with molecular orbital interactions between donors and acceptors of halogen bonds, which indicates the importance of the covalent component in the binding of halogens.

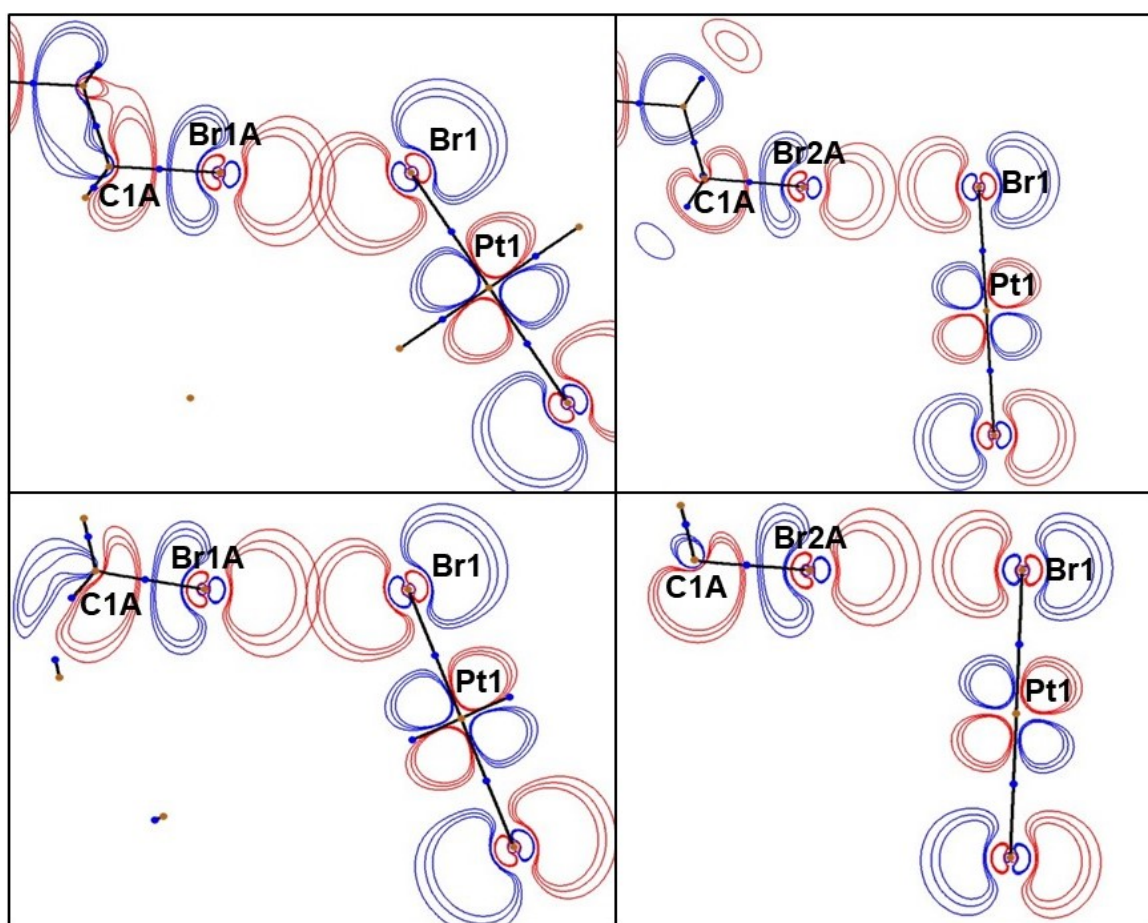


Figure 6. HOMO-LUMO overlap projections for XBs Br1A...Br1 and Br2A...Br1 in 1-tbe (top) and in 2-tbe (bottom).

4. Conclusions

In this work, we firstly found the formation of XBs with 1,1,2,2-tetrabromoethane as XB donor, which were shown in the formation of 1:1 solvates with platinum(II) bromide dialkylcyanamide complexes. The nature of halogen bonds was investigated experimentally by single-crystal X-ray diffraction analysis of the solvates. Further theoretical calculations, including topological analysis of electron density, ESP surfaces, ELF projections, HOMO/LUMO overlaps, Wiberg bond indices and natural population charge analysis, confirmed tetrabromoethane is indeed an electrophile toward bromide ligand due to the presence of σ -holes on bromine atoms. As other bromoalkanes, it can be used as electrophilic supramolecular synthon (donor of four σ -holes) together with bromide complexes.

Our inspection of literature data for substances with the general formula $RCHBr_2$ show that they may also be studied as potential XB donors [51–56], among dibromomethane, bromoform and 1,1,2,2-tetrabromoethane.

Supplementary Materials: The following are available online at <https://www.mdpi.com/article/10.3390/cryst11070835/s1>, Figure S1: Structure of complex $trans-[PtBr_2(NCN(CH_2)_5)_2]$; Figure S2: Formation of 2D polymer networks in adducts **1·tbe** (top) and **2·tbe** (bottom); Figure S3: IR-spectra of complex $trans-[PtBr_2(NCN(CH_2)_5)_2]$: 2944 (w), 2852 (w), $\nu(C-H)$; 2291 (s), $\nu(C\equiv N)$; 1170 (w), 1107 (w), $\nu(C-N)$; 467 (m), $\nu(Pt-N)$; Figure S4: Mass spectrum of complex $trans-[PtBr_2(NCN(CH_2)_5)_2]$; Figure S5: 1H NMR spectrum of complex $trans-[PtBr_2(NCN(CH_2)_5)_2]$; Figure S6: $^{13}C\{^1H\}$ NMR spectrum of complex $trans-[PtBr_2(NCN(CH_2)_5)_2]$; Figure S7: ^{195}Pt NMR spectrum of complex $trans-[PtBr_2(NCN(CH_2)_5)_2]$; Figure S8: Comparison of PXRD (red line) and XRD (blue line) complex $trans-[PtBr_2(NCN(CH_2)_5)_2]$. The phases coincide, the difference is due to different experimental conditions (for PXRD—RT, for XRD—100 K). Figure S9: Structure of cluster **1·tbe** (halogen bonding); Figure S10: Structure of cluster **1·tbe** (hydrogen bonding); Figure S11: Structure of cluster **2·tbe** (halogen bonding). Table S1: Crystal data and structure refinement for **1·tbe**, **2** and **2·tbe** at 100 K; Table S2: Values of the Wiberg indices (WBI), Lagrangian kinetic energy $G(r)$, potential energy density $V(r)$ and energy density $H(r)$ (Hartree) at the bond critical points (3, -1), corresponding to different noncovalent interactions in **1·tbe**.

Author Contributions: A.M.C.—writing, investigation and computational study; D.M.I.—writing, computational study, conceptualization and project administration. All authors have read and agreed to the published version of the manuscript.

Funding: The research was supported by Ministry of Science and Higher Education of the Russian Federation in frame of “Mega-grant project” (075-15-2021-585).

Institutional Review Board Statement: Not applicable.

Informed Consent Statement: Not applicable.

Data Availability Statement: Data are available from the corresponding author on request.

Acknowledgments: The author thanks the resource centers of St. Petersburg State University “Centre for X-ray Diffraction Studies”, “Chemical Analysis and Materials Research Centre” and “Magnetic Resonance Research Centre” for their support in the research. Special thanks to V. Yu. Kukushkin for help in writing of the article.

Conflicts of Interest: The authors declare no conflict of interest.

References

1. Desiraju, G.R.; Ho, P.S.; Kloo, L.; Legon, A.C.; Marquardt, R.; Metrangolo, P.; Politzer, P.; Resnati, G.; Rissanen, K. Definition of the halogen bond (IUPAC Recommendations 2013). *Pure Appl. Chem.* **2013**, *85*, 1711–1713. [CrossRef]
2. Berger, G.; Frangville, P.; Meyer, F. Halogen bonding for molecular recognition: New developments in materials and biological sciences. *Chem. Commun.* **2020**, *56*, 4970–4981. [CrossRef]
3. Cavallo, G.; Metrangolo, P.; Milani, R.; Pilati, T.; Priimagi, A.; Resnati, G.; Terraneo, G. The Halogen Bond. *Chem. Rev.* **2016**, *116*, 2478–2601. [CrossRef]
4. Mukherjee, A.; Tothadi, S.; Desiraju, G.R. Halogen bonds in crystal engineering: Like hydrogen bonds yet different. *Acc. Chem. Res.* **2014**, *47*, 2514–2524. [CrossRef]
5. Politzer, P.; Lane, P.; Concha, M.C.; Ma, Y.; Murray, J.S. An overview of halogen bonding. *J. Mol. Model.* **2007**, *13*, 305–311. [CrossRef]
6. Cavallo, G.; Metrangolo, P.; Pilati, T.; Resnati, G.; Sansotera, M.; Terraneo, G. Halogen bonding: A general route in anion recognition and coordination. *Chem. Soc. Rev.* **2010**, *39*, 3772–3783. [CrossRef]
7. Nemeč, V.; Lisac, K.; Bedeković, N.; Fotović, L.; Stilinović, V.; Cinčić, D. Crystal engineering strategies towards halogen-bonded metal–organic multi-component solids: Salts, cocrystals and salt cocrystals. *CrystEngComm* **2021**, *23*, 3063–3083. [CrossRef]
8. Brammer, L.; Mínguez Espallargas, G.; Libri, S. Combining metals with halogen bonds. *CrystEngComm* **2008**, *10*, 1712–1727. [CrossRef]
9. Bertani, R.; Sgarbossa, P.; Venzo, A.; Lelj, F.; Amati, M.; Resnati, G.; Pilati, T.; Metrangolo, P.; Terraneo, G. Halogen bonding in metal–organic–supramolecular networks. *Coord. Chem. Rev.* **2010**, *254*, 677–695. [CrossRef]
10. Li, B.; Zang, S.-Q.; Wang, L.-Y.; Mak, T.C.W. Halogen bonding: A powerful, emerging tool for constructing high-dimensional metal-containing supramolecular networks. *Coord. Chem. Rev.* **2016**, *308*, 1–21. [CrossRef]

11. Farina, A.; Meille, S.V.; Messina, M.T.; Metrangolo, P.; Resnati, G.; Vecchio, G. Resolution of Racemic 1,2-Dibromohexafluoropropane through Halogen-Bonded Supramolecular Helices. *Angew. Chem. Int. Ed.* **1999**, *38*, 2433–2436. [CrossRef]
12. Rosokha, S.V.; Stern, C.L.; Ritzert, J.T. Experimental and computational probes of the nature of halogen bonding: Complexes of bromine-containing molecules with bromide anions. *Chem. A Eur. J.* **2013**, *19*, 8774–8788. [CrossRef] [PubMed]
13. Rosokha, S.V.; Traversa, A. From charge transfer to electron transfer in halogen-bonded complexes of electrophilic bromocarbons with halide anions. *Phys. Chem. Chem. Phys.* **2015**, *17*, 4989–4999. [CrossRef] [PubMed]
14. Kashina, M.V.; Kinzhalov, M.A.; Smirnov, A.S.; Ivanov, D.M.; Novikov, A.S.; Kukushkin, V.Y. Dihalomethanes as bent bifunctional XB/XB-donating building blocks for construction of metal-involving halogen bonded hexagons. *Chem. Asian J.* **2019**, *14*, 3915–3920. [CrossRef]
15. Ivanov, D.M.; Novikov, A.S.; Starova, G.L.; Haukka, M.; Kukushkin, V.Y. A family of heterotetrameric clusters of chloride species and halomethanes held by two halogen and two hydrogen bonds. *CrystEngComm* **2016**, *18*, 5278–5286. [CrossRef]
16. Rosokha, S.V.; Vinakos, M.K. Hybrid network formation via halogen bonding of the neutral bromo-substituted organic molecules with anionic metal–bromide complexes. *Cryst. Growth Des.* **2012**, *12*, 4149–4156. [CrossRef]
17. Baykov, S.V.; Dabranskaya, U.; Ivanov, D.M.; Novikov, A.S.; Boyarskiy, V.P. Pt/Pd and I/Br Isostructural Exchange Provides Formation of C–I···Pd, C–Br···Pt, and C–Br···Pd Metal-Involving Halogen Bonding. *Cryst. Growth Des.* **2018**, *18*, 5973–5980. [CrossRef]
18. Dabranskaya, U.; Ivanov, D.M.; Novikov, A.S.; Matveychuk, Y.V.; Bokach, N.A.; Kukushkin, V.Y. Metal-Involving Bifurcated Halogen Bonding C–Br···η²(Cl–Pt). *Cryst. Growth Des.* **2019**, *19*, 1364–1376. [CrossRef]
19. Rosokha, S.V.; Lu, J.; Rosokha, T.Y.; Kochi, J.K. Halogen-bonded assembly of hybrid inorganic/organic 3D-networks from dibromocuprate salts and tetrabromomethane. *Chem. Commun.* **2007**, 3383–3385. [CrossRef]
20. Fuller, R.O.; Griffith, C.S.; Koutsantonis, G.A.; Lapere, K.M.; Skelton, B.W.; Spackman, M.A.; White, A.H.; Wild, D.A. Supramolecular interactions between hexabromoethane and cyclopentadienyl ruthenium bromides: Halogen bonding or electrostatic organisation? *CrystEngComm* **2012**, *14*, 804–811. [CrossRef]
21. Nudnova, E.A.; Potapov, A.S.; Khlebnikov, A.I.; Ogorodnikov, V.D. Synthesis of ditopic ligands containing bis(1H-pyrazol-1-yl)-methane fragments. *Russ. J. Org. Chem.* **2007**, *43*, 1698–1702. [CrossRef]
22. Krajenta, A.; Rozanski, A. Physical state of the amorphous phase of polypropylene-influence on thermo-mechanical properties. *Polymer* **2015**, *70*, 127–138. [CrossRef]
23. Sünkel, K.; Bernhartzeder, S. Coordination chemistry of perhalogenated cyclopentadienes and alkynes. XXVIII [1] new high-yield synthesis of monobromoferrocene and simplified procedure for the synthesis of pentabromoferrocene. Molecular structures of 1,2,3-tribromoferrocene and 1,2,3,4,5-pentabromoferrocene. *J. Organomet. Chem.* **2011**, *696*, 1536–1540. [CrossRef]
24. Butler, I.R.; Woldt, B.; Oh, M.-Z.; Williams, D.J. Ferrocene pincer ligands made easy. *Inorg. Chem. Commun.* **2006**, *9*, 1255–1258. [CrossRef]
25. Cowie, B.E.; Emslie, D.J.H. Platinum Complexes of a Borane-Appended Analogue of 1,1'-Bis(diphenylphosphino)ferrocene: Flexible Borane Coordination Modes and in situ Vinylborane Formation. *Chem. A Eur. J.* **2014**, *20*, 16899–16912. [CrossRef]
26. Inkpen, M.S.; Du, S.; Driver, M.; Albrecht, T.; Long, N.J. Oxidative purification of halogenated ferrocenes. *Dalton Trans.* **2013**, *42*, 2813–2816. [CrossRef]
27. Shafir, A.; Power, M.P.; Whitener, G.D.; Arnold, J. Synthesis, structure and properties of 1,1'-diamino- and 1,1'-diazidoferrocene. *Organometallics* **2000**, *19*, 3978–3982. [CrossRef]
28. Fulton, J.D. XXIX.—Action of acetylene tetrabromide on organic bases. *J. Chem. Soc.* **1926**, *129*, 197–199. [CrossRef]
29. Ivanov, D.M.; Novikov, A.S.; Ananyev, I.V.; Kirina, Y.V.; Kukushkin, V.Y. Halogen bonding between metal centers and halocarbons. *Chem. Commun.* **2016**, *52*, 5565–5568. [CrossRef] [PubMed]
30. Sheldrick, G. SHELXT-integrated space-group and crystal-structure determination. *Acta Crystallogr. Sect. A* **2015**, *71*, 3–8. [CrossRef] [PubMed]
31. Sheldrick, G. A short history of SHELX. *Acta Crystallogr. Sect. A* **2008**, *64*, 112–122. [CrossRef]
32. Weigend, F. Accurate Coulomb-fitting basis sets for H to Rn. *Phys. Chem. Chem. Phys.* **2006**, *8*, 1057–1065. [CrossRef]
33. Pollak, P.; Weigend, F. Segmented contracted error-consistent basis sets of double- and triple-ζ valence quality for one- and two-component relativistic all-electron calculations. *J. Chem. Theory Comput.* **2017**, *13*, 3696–3705. [CrossRef]
34. Frish, M.J.; Scuseria, G.E.; Robb, M.A.; Cheeseman, J.R.; Scalmani, G.; Barone, V.; Mennucci, B.; Petersson, G.A.; Nakatsuji, H.; Caricato, M.; et al. Gaussian09W. 2009. Available online: <http://www.gaussian.com/> (accessed on 30 December 2013).
35. Scrocco, E.; Tomasi, J. *The Electrostatic Molecular Potential as a Tool for the Interpretation of Molecular Properties*; Springer: Berlin/Heidelberg, Germany, 1973; Volume 42, pp. 95–170. [CrossRef]
36. Humphrey, W.; Dalke, A.; Schulten, K. VMD: Visual molecular dynamics. *J. Mol. Graph.* **1996**, *14*, 33–38. [CrossRef]
37. Lu, T.; Chen, F. Multiwfn: A multifunctional wavefunction analyzer. *J. Comput. Chem.* **2012**, *33*, 580–592. [CrossRef]
38. Perrin, C.L. Atomic size dependence of Bader electron populations: Significance for questions of resonance stabilization. *J. Am. Chem. Soc.* **1991**, *113*, 2865–2868. [CrossRef]
39. Toikka, Y.N.; Mikherdov, A.S.; Ivanov, D.M.; Mooibroek, T.J.; Bokach, N.A.; Kukushkin, V.Y. Cyanamides as π-hole donor components of structure-directing (cyanamide)···arene noncovalent interactions. *Cryst. Growth Des.* **2020**, *20*, 4783–4793. [CrossRef]

40. Eliseeva, A.A.; Ivanov, D.M.; Rozhkov, A.V.; Ananyev, I.V.; Frontera, A.; Kukushkin, V.Y. Bifurcated Halogen Bonding Involving Two Rhodium(I) Centers as an Integrated σ -Hole Acceptor. *JACS Au* **2021**, *1*, 354–361. [[CrossRef](#)]
41. Bondi, A. van der Waals Volumes and Radii. *J. Phys. Chem.* **1964**, *68*, 441–451. [[CrossRef](#)]
42. Metrangolo, P.; Resnati, G. Type II halogen . . . halogen contacts are halogen bonds. *IUCr* **2014**, *1*, 5–7. [[CrossRef](#)] [[PubMed](#)]
43. Tupikina, E.Y.; Bodensteiner, M.; Tolstoy, P.M.; Denisov, G.S.; Shenderovich, I.G. P=O Moiety as an Ambidextrous Hydrogen Bond Acceptor. *J. Phys. Chem. C* **2018**, *122*, 1711–1720. [[CrossRef](#)]
44. Bader, R.F.W.; Nguyen-Dang, T.T. Quantum Theory of Atoms in Molecules–Dalton Revisited. In *Advances in Quantum Chemistry*; Löwdin, P.-O., Ed.; Academic Press: Cambridge, MA, USA, 1981; Volume 14, pp. 63–124.
45. Bader, R.F.W. A quantum theory of molecular structure and its applications. *Chem. Rev.* **1991**, *91*, 893–928. [[CrossRef](#)]
46. Johnson, E.R.; Keinan, S.; Mori-Sánchez, P.; Contreras-García, J.; Cohen, A.J.; Yang, W. Revealing Noncovalent Interactions. *J. Am. Chem. Soc.* **2010**, *132*, 6498–6506. [[CrossRef](#)]
47. Becke, A.D.; Edgecombe, K.E. A simple measure of electron localization in atomic and molecular systems. *J. Chem. Phys.* **1990**, *92*, 5397–5403. [[CrossRef](#)]
48. Yushina, I.D.; Kolesov, B.A. Interplay of intra- and intermolecular interactions in solid iodine at low temperatures: Experimental and theoretic spectroscopy study. *J. Phys. Chem. A* **2019**, *123*, 4575–4580. [[CrossRef](#)] [[PubMed](#)]
49. Lyssenko, K.A.; Grintselev-Knyazev, G.V.; Antipin, M.Y. Nature of the PO bond in diphenylphosphonic acid: Experimental charge density and electron localization function analysis. *Mendeleev Commun.* **2002**, *12*, 128–130. [[CrossRef](#)]
50. Rosokha, S.V.; Stern, C.L.; Swartz, A.; Stewart, R. Halogen bonding of electrophilic bromocarbons with pseudohalide anions. *Phys. Chem. Chem. Phys.* **2014**, *16*, 12968–12979. [[CrossRef](#)] [[PubMed](#)]
51. Gou, G.-Z.; Kou, J.-F.; Zhou, Q.-D.; Chi, S.-M. N-(7-Dibromomethyl-5-methyl-1,8-naphthyridin-2-yl)acetamide-pyrrolidine-2,5-dione. *Acta Crystallogr. Sect. E* **2013**, *69*, o153–o154. [[CrossRef](#)] [[PubMed](#)]
52. Vande Velde, C.M.L.; Zeller, M.; Azov, V.A. Comparison of computationally cheap methods for providing insight into the crystal packing of highly bromomethylated azobenzenes. *Acta Crystallogr. Sect. C* **2018**, *74*, 1692–1702. [[CrossRef](#)]
53. Liu, X.; Kilner, C.A.; Thornton-Pett, M.; Halcrow, M.A. 1-(Dibromomethyl)-4-methoxy-2-methylbenzene. *Acta Crystallogr. Sect. C* **2001**, *57*, 317–318. [[CrossRef](#)]
54. Gayathri, K.; Mohan, P.S.; Howard, J.A.K.; Sparkes, H.A. Crystal structure of 3-bromomethyl-2-chloro-6-(dibromomethyl)quinoline. *Acta Crystallogr. Sect. E* **2015**, *71*, o354–o355. [[CrossRef](#)] [[PubMed](#)]
55. Rosin, R.; Seichter, W.; Mazik, M. Crystal structures of the dioxane hemisolvates of N-(7-bromomethyl-1,8-naphthyridin-2-yl)acetamide and bis[N-(7-dibromomethyl-1,8-naphthyridin-2-yl)acetamide]. *Acta Crystallogr. Sect. E* **2017**, *73*, 1409–1413. [[CrossRef](#)] [[PubMed](#)]
56. Fun, H.K.; Goh, J.H.; Chandrakantha, B.; Isloor, A.M. 1-Dibromo-methyl-4-methoxy-2-nitro-benzene. *Acta Crystallogr. Sect. E Struct. Rep. Online* **2009**, *65*, o2193–o2194. [[CrossRef](#)] [[PubMed](#)]